Original Research Article
Construction of a 3D conceptual model of subsurface sulfide mineralizations using integrated geophysical survey in Saint Catherine, South Sinai, Egypt

.

ABSTRACT

The genesis and mode of occurrence of sulfide mineralizations located within the quartz monzonite rocks of Saint Catherine Area, Egypt have divided researchers who studied them into 2 main groups. One group believes that the mineralizations belong to the porphyry copper type of deposits, while the other group thinks that the mineralizations are formed by deposition of sulfides-rich hydrothermal solution in the structural lineaments. We conducted an integrated geophysical survey using magnetic, radiometric, very low frequency and turam electromagnetic methods to solve this conflict. Incorporating the results of the geophysical surveys with the previously available geological and geochemical data helps building up a realistic conceptual 3D model of the subsurface sulfide mineralizations. The model proposes that the mineralizations are formed through 2 stages of upward migration of hydrothermal solutions. The early stage resulted in the deposition of a deep massive heap of mineralizations, creating features that support porphyry copper deposits. In the later stage, some of these hydrothermal solutions traveled farther upward, along fault planes and dykes, forming shallower linear mineralized deposits controlled by the NW-SE structural lineaments. Both mineral deposits were deformed, displaced, and dissected by faults and dykes trending NE-SW, creating the present complicated situation, and showing contradicting evidences on their mode of occurrence. The proposed conceptual model accommodates all previously introduced evidences, solves the conflict between existing contradicting hypotheses, and presents a reasonable evidence-based view of the geometry and mode of formation of these mineralizations.

Keywords: 3D model, magnetic, very-low frequency, turam, gamma ray spectrometry

1. INTRODUCTION

Subsurface sulfide mineralizations; located within the altered quartz monzonite rocks near Saint Catherine City, south Sinai, Egypt; have been subjected to intensive investigations during the past 4 decades [1-10]. The presence of subsurface mineralizations has been well proven, however, the mode of formation and subsurface layout of these mineralizations are still debatable. A group of previous studies state that the presence of disseminated porphyry copper related minerals are supporting evidence for porphyry copper mineralization [3, 11]. Moreover, the intense alteration shattering near peripheral zones and the porphyry texture of the quartz monzonite rocks are considered good geological criteria of such type of mineralization [12]. On the other hand, the alignment of concentrated subsurface mineralizations with major structural elements in the area as well as the presence of surface

mineralization showings within the fresh quartz monzonite rocks raise doubts about the porphyry copper theory. These doubts have led another group of researchers to conclude that subsurface mineralizations are formed by hydrothermal solutions depositing along the structural lineaments in the area. Some researchers stated that mineralizations are controlled by structural elements trending NE-SW [1], while others claimed that they are related to faults and dykes trending NW-SE and WNW-ESE direction [2]. Recently acquired evidences stated that both previously mentioned directions can be associated with mineralizations in South Sinai [13].

Other studies could not reach a concrete conclusion about the source of the mineralizations in Saint Catherine area, stating that the surface showings can be a result of weak porphyry copper style alteration or multiple weak hydrothermal events [14]. Recently, yet another model, that relates these mineralizations to post-ring dyke formation volcanic activities within the ring dykes, has been introduced [8].

The aim of this study is to use the results of our multiple coincident geophysical survey to build up a new conceptual model that solves the dispute among the previously mentioned hypotheses and explains the genesis and subsurface layout of sulfide mineralizations in Saint Catherine area.

2. STUDY AREA

The study area lies to the east of Saint Catherine City in the central south of Sinai Peninsula and is mainly covered by granitic rocks that belong to the Precambrian basement of the northern part of the Arabo-Nubian Shield (Fig. 1).

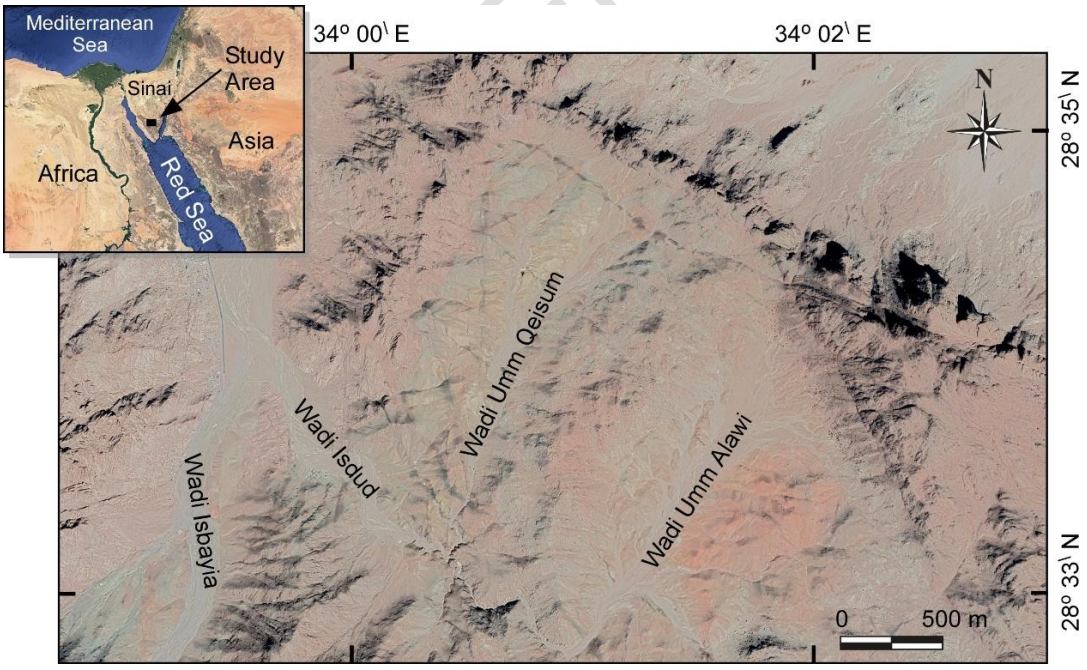

Fig. 1. Landsat image of the study area

A highly altered area lies in the northwestern corner of a large quartz monzonite pluton. This area is bounded to the west by alkali feldspar granite and to the east by fresh quartz monzonite. The northeastern side of the altered area is bounded by quartz syenite rocks that form a segment of a huge ring dyke surrounding the entire Saint Catherine area (Fig. 2).

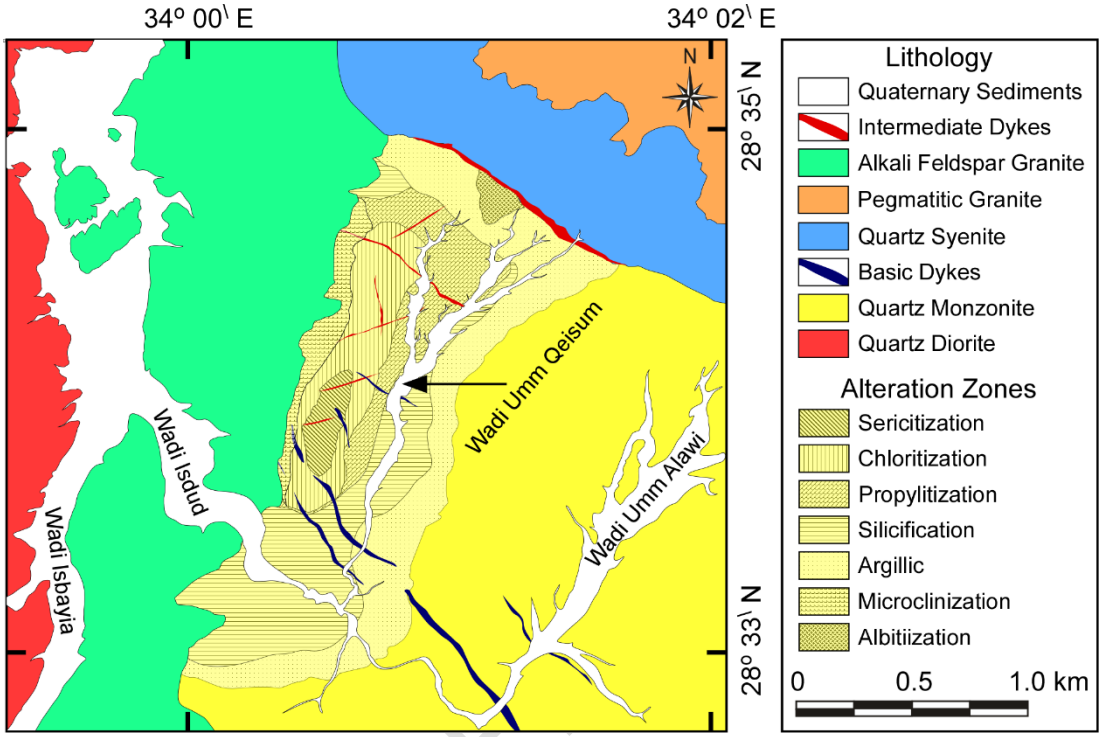

Fig. 2. Geologic map of the study area showing the lithology and alteration zones

Within the highly altered area, seven irregular concentric and overlapped alteration zones were detected [15]. These alteration zones, arranged from the center outwards, are the sericitization, chloritization, propylitization, silicification, argillic, microclination and albitization zones. The presence of these alteration zones and the geologic setting of the quartz monzonite rocks in addition to the porphyry texture of the quartz monzonite were believed to be good geological criteria of porphyry copper mineralization [12].

The study area is dissected by several structural lineaments trending in different directions; however, two major sets of faults form the main structural elements. The first set forms a group of long parallel fault planes trending parallel to the Gulf of Aqaba in the NE-SW and NNE-SSW directions. The other set is parallel to the Gulf of Suez in the WNW-ESE direction. Another group of faults runs in the N-S direction, with less frequency than the previously mentioned two main directions (Fig. 2).

Geochemical analyses of the groundwater, quaternary stream sediments and bedrock samples collected from the area show anomalous amounts of many sulfide minerals, including pyrite, nawackite, chalcopyrite and bornite [11].

3. METHODOLOGY

A coincident multiple geophysical survey is conducted to investigate the highly altered quartz monzonite zone and its contact with surrounding rocks. This survey employs Vertical Magnetic Gradient (VGM), gamma-ray spectrometry, very low frequency electromagnetic (VLF-EM), and turam methods (Fig. 3). The field geophysical measurements are collected coincidently along 8 profiles trending NE-SW with a profile separation of 120 m. The profiles orientations are adjusted to intersect the main structural trends associated with surface showings of mineralization and to allow good reception of the VLF-EM signal. Field tests conducted on the area prior to the survey show that no fixed station interval can be adequate for all the four geophysical methods. The main advantage of using several geophysical methods coincidently is the capability to image different physical properties at different depths of the subsurface within the surveyed area. This may allow for acquiring several consecutive depth slices of the subsurface mineralizations.

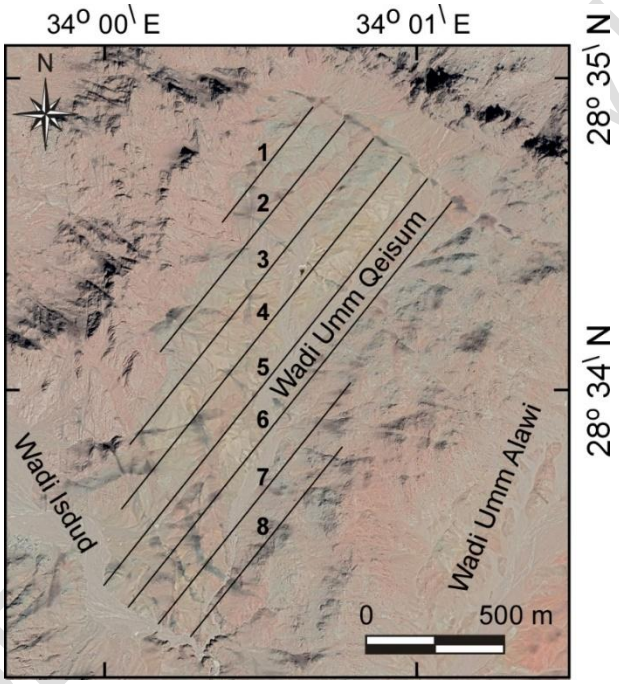

Fig. 3. Geophysical survey layout in the study area

Vertical magnetic gradient and very low frequency measurements would provide a general overview of the vertical and horizontal layout of the subsurface sulfide mineralizations, while multi-frequency turam measurements present virtual depth slices of these mineralizations. Finally, gamma-ray spectrometry would explain the lateral distribution of the radioelements characterizing the quartz monzonite pluton, which would complete the image and facilitate the construction of the conceptual model.

The VMG data are collected using a fluxgate magnetometer (MFD-4), which is designed to measure the vertical component of the earth's magnetic field. At every station, the magnetic readings are measured, at heights of 50 and 120 cm, along the previously mentioned 8 profiles using a constant station interval of 50 m. The vertical magnetic gradient (VMG) values are calculated based to the following equation:

$$VMG = (Z2 - Z1)/\Delta h \quad (1)$$

where Z1 is the magnetic reading at height h1, Z2 is the magnetic reading at a height h2 and Δh is (h2 – h1).

Whenever an abrupt change in readings is noticed, this station interval is reduced to 25 m or less to accommodate such changes. The collected data are subjected to appropriate processing routine and vertical magnetic gradient values are gridded and presented as a contour map and 3D surface map (Fig. 4). The purpose of this magnetic survey is to shed some light on the major geologic structures and lineaments, where subsurface mineralizations may be concentrated.

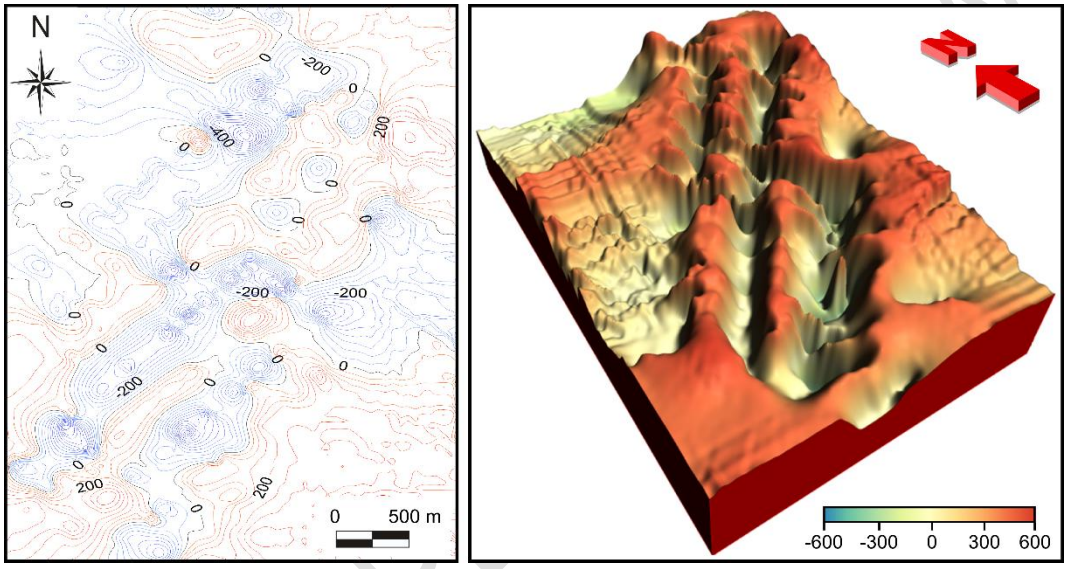

Fig. 4. Vertical magnetic gradient contour map (left) and 3D surface map (right)

VLF-EM method is one of the most effective geophysical tools to investigate subsurface mineralizations, in general, and sulfides, in particular [16]. The VLF-EM data are collected using a single-coil receiver (SCOPAS SE-81), which is capable of measuring both the horizontal and vertical magnetic components of the resultant electromagnetic field in addition to the tilt angle. The signal received from the Russian Radio Broadcasting Station (RBU) at Moscow, with a frequency of 66.666 kHz and radiating power of 10 kW, is used to collect the VLF-EM data along the 8 profiles. Based on field tests, a station interval of 50 m is found adequate for this survey.

The collected tilt angle values are corrected to remove the topographic effect by applying Eberle technique [17]. These corrected values are filtered using Fraser technique to transfer the inflection points on the tilt angle profiles into positive peaks and then the percentage real component values are calculated [18]. These real component values are gridded and plotted as a contour map and 3D surface map (Fig. 5). Profiles are drawn perpendicular to the short axes of anomalous regions of interest on both the VGM and VLF contour maps. The depths to the subsurface bodies causing these anomalies are calculated from these profiles using a combination of simple depth estimation methods. The commonly used half-width method, modified straight-slope method [19], and Smith Rules method [20] are applied to each

anomaly. The results are the 3 methods are averaged to achieve an accurate depth estimation of the causative body.

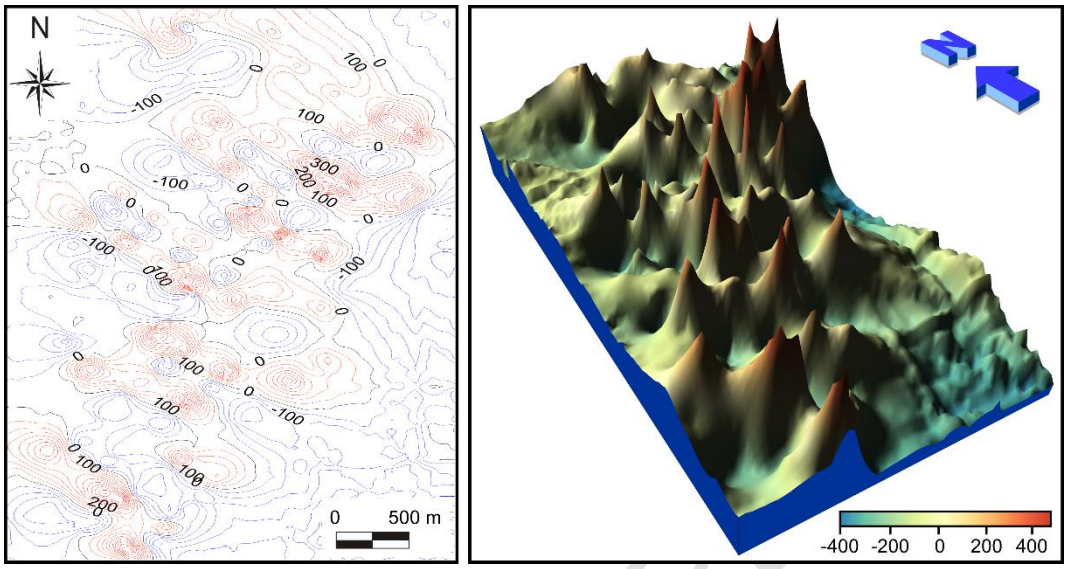

Fig. 5. VLF-EM real component contour map (left) and 3D surface map (right)

The relationship between concentration of potassic alteration and porphyry copper deposits is well established [21-23]. A gamma ray spectrometry survey is conducted to investigate the concentration of potassium in the study area. This survey is conducted using a digital, four-channel, gamma-ray spectrometer (GAD-6). This device is used to measure the counts per second of potassium, thorium, and uranium in addition to the total count along the assigned profiles using a station interval of 20 meters. The collected data are then converted into radioelement concentrations and the potassium/thorium ratio is then calculated, gridded, and plotted as a contour map and a 3D surface map (Fig. 6).

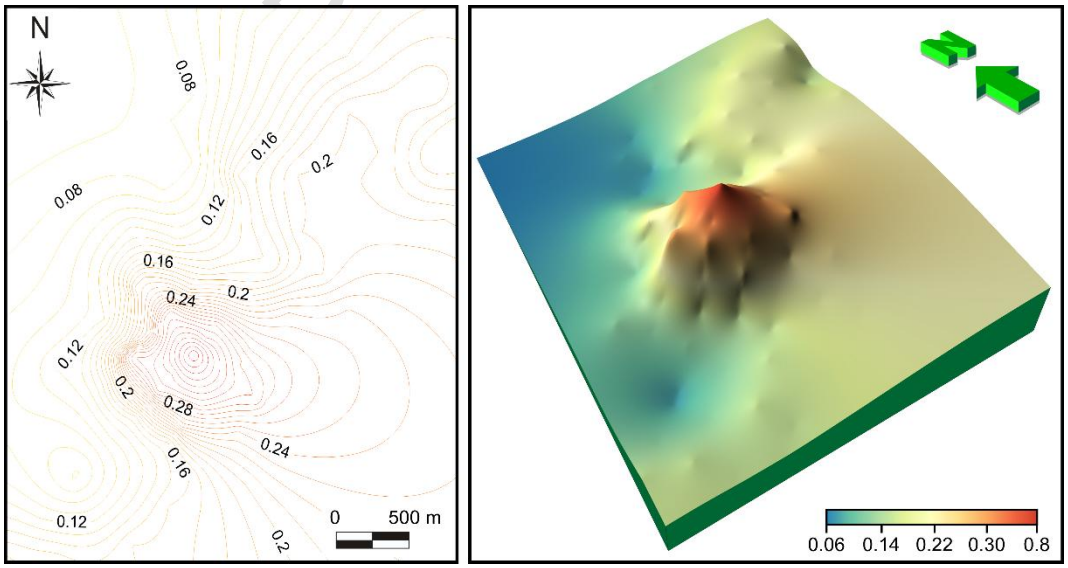

Fig. 6. Potassium/thorium ratio contour map (left) and 3D surface map (right)

The turam-EM method is one of the most powerful and effective electromagnetic tools for subsurface mineralization in rough terrain areas. A turam-EM system (SE-71), which measures both field strength ratio (FSR) and phase difference (PD), is used to collect field data at 3 frequencies; that are 200, 400 and 800 Hz. The turam field survey is divided into parts. In the first part, a regional survey covers the highly altered area of the quartz monzonite rocks as well as its contact with adjacent rocks (Fig. 2). The turam profiles are measured around each transmitter loop using the TX-parallel configuration [24]. This configuration is selected to allow turam profiles to be coincident with the rest of geophysical profiles in the area. The collected FSR and PD measurements are normalized to remove the effect of the end of loop and to correct the distortion in the FSR values near the edges of the transmitter loops. After the normalization process, the real (R) and imaginary (I) components of the resultant field are calculated. Figure 7 shows a contour map and a 3D surface map of the field strength ratio acquired using frequency of 800 Hz, while figure 8 shows a contour map and a 3D surface map of the field strength ratio on frequency of 200 Hz. The results of frequency of 400 Hz are not displayed here because they show no new features other than those displayed in figures 7 and 8.

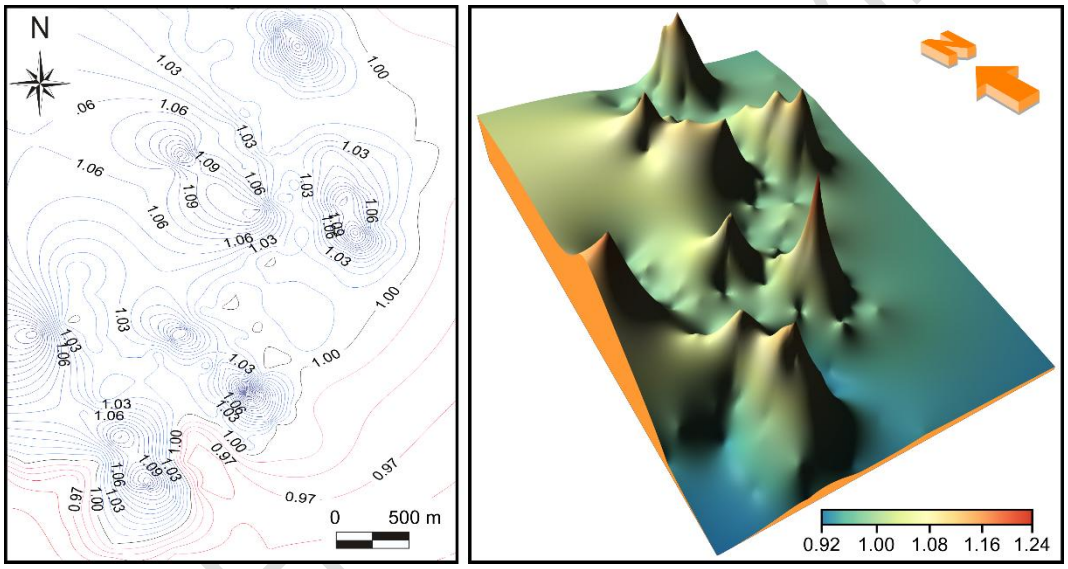

Fig. 7. Turam field strength ratio (800 Hz) contour map (left) and 3D surface map (right)

The results of the regional turam survey yielded some interesting phenomenon in the southcentral part of the highly altered zone that should be investigated in detail by further turam measurements. The interesting site is surveyed using smaller profile spacing and station interval to get a magnified view of the distribution of deep subsurface sulfide bodies in this region. In this part, one transmitter loop with a length of 1300 m and a width of 200 m is laid out on the terrain in order to survey the site of interest. Both FSR and PD are measured along eight TX-profiles around the loop. These profiles are trending N 40o E and their lengths varied from 550 to 850 m, based on the topography of the surveyed area. At this part, a profile separation of 50 m and station interval of 15 m are found adequate. The collected measurements are processed using the same processing routine explained earlier and the processed FSR values are gridded and plotted as a contour map and a 3D surface map (Fig. 9). The depth estimation of turam measurements is conducted using the TUMOD software [25]. The software employs curve matching, based on a line current approximation, between collected and theoretically computed values of FSR and PD. Manual manipulation

of current axes parameters are performed until a best fit between the collected and the computed curves is achieved, which provides precise depth estimation of turam anomalies.

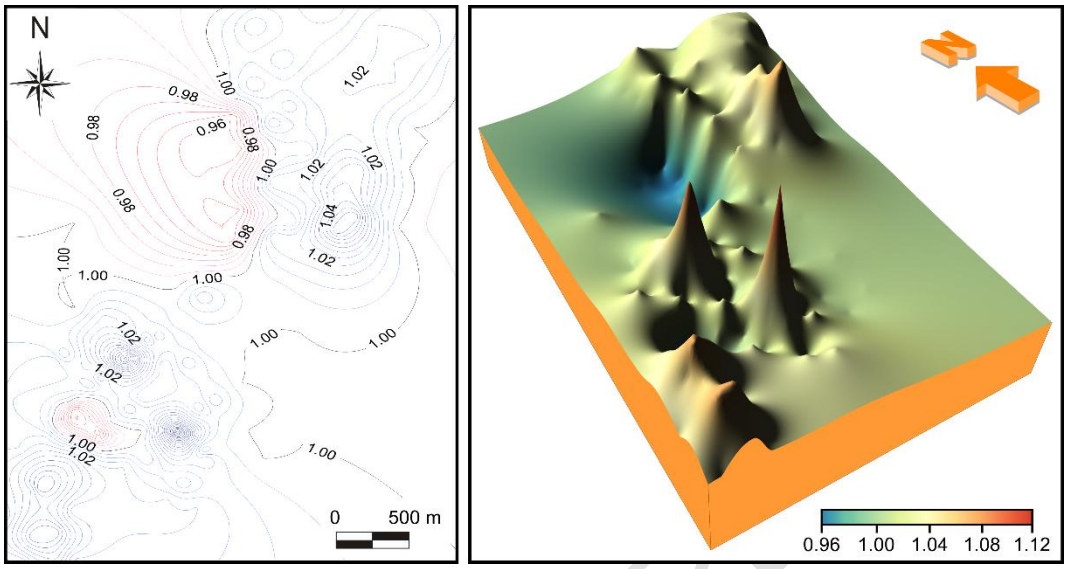

Fig. 8. Turam field strength ratio (200 Hz) contour map (left) and 3D surface map (right)

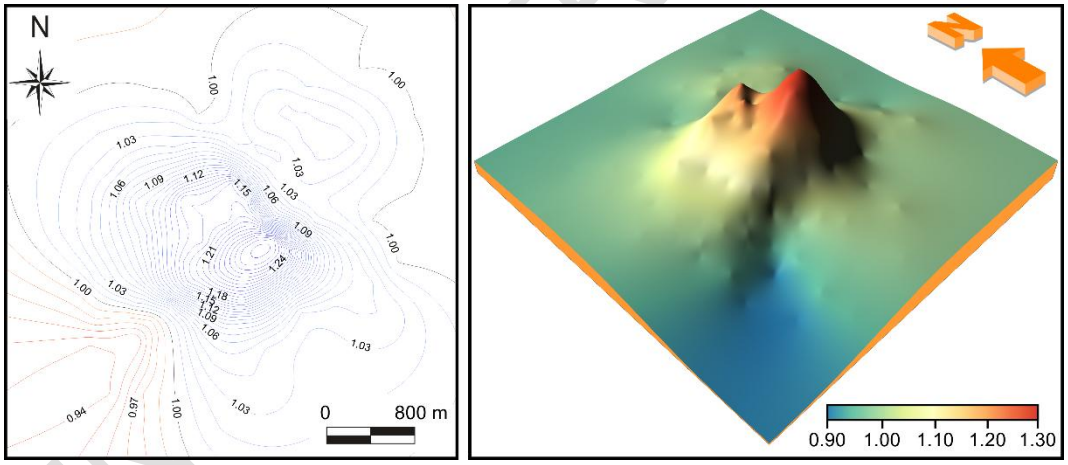

Fig. 9. Detailed turam field strength ratio (200 Hz) contour map (left) and 3D surface map (right)

4. RESULTS AND DISCUSSION

The vertical magnetic gradient survey reveals the presence of several anomalies in the highly altered zone of the quartz monzonite rocks of the study area. Two major long anomalies are trending NE-SW. These anomalies are intersected by several elongated perpendicular anomalies trending in the NW-SE direction (Fig. 4). The contour map shows both trends, while the 3D surface map shows their trends, sizes, and intersections in a much better way. The estimated depth of a representative group of these anomalies indicates

ranges between 30 and 70 m below the ground surface. Moreover, the distribution of the magnetic anomalies over the area is fairly uniform with no specific concentration spots. This may encourage leaning towards the structurally controlled subsurface mineralization theory.

The VLF-EM anomaly contour map and 3D surface map show clear similarity to features found on the vertical magnetic gradient map. The two major trends of NE-SW and NW-SE are quite clear on the contour map. The NW-SE trend, however, is more dominant and abundant than the NE-SW trend. This may be attributed to the broadcasting direction of the Russian broadcasting station that may emphasize the NW-SE direction anomalies more, because they are perpendicular to the primary signal direction. On the other hand, most of the detected VLF-EM anomalies are spatially coincident with those of the vertical magnetic gradient ones. Most VLF-EM anomalies are also oval with their long axes trending in the NW-SE direction, which can be seen clearly on the contour map (Fig. 5). The depths estimated for the causative sulfide bodies range between 25 and 82 m below the ground surface. The large intensity and uniform distribution of the VLF-EM anomalies indicate the presence of shallow subsurface mineralization concentrations that are coincident with the structural elements interpreted from the vertical magnetic gradient maps. The even distribution of anomalies and their irrelevance to any of the alteration zones, shown in Figure 2, can be clearly seen on both the contour map and the 3D surface map of the real component VLF-EM. These findings are in favor of the structurally controlled mineralization model.

Potassium/thorium ratio map shows a single, large, semi-rounded anomaly in the south-central part of the highly altered area. This anomaly is slightly elongated in the NW-SE direction (Fig. 6). The long axis of this anomaly coincides with a major fault deduced from the vertical magnetic gradient map. The rest of the surveyed area shows either relatively low flat contours, as in the fresh quartz monzonite located on the southeast of the surveyed area or very low ratios, such as in the northwestern corner. This large anomaly is closely related to the surface alteration zones. The anomaly also indicates a focused hydrothermal activity in close approximation to the detected alteration zones. Both potassium and thorium radio elements accompany sulfide mineralization originated from hydrothermal activity. Because potassium is relatively more stable than thorium, in time, continuous leaching process causes the potassium/thorium ratio to increase. This increase is usually gradual towards the center of the anomaly. The presence of such anomaly and its spatial relation to the alteration zones indicate a single large hydrothermal activity that is spatially coincident with the highly altered area. This may appear as contradicting evidence of the information depicted earlier from the VGM and VLF-EM data.

Among all geophysical methods, turam-EM is best way to detect and trace subsurface mineralization in an accurate and precise way. Because field data can be collected using different frequencies, virtual depth slices can be acquired. As the frequency decreases, the electromagnetic waves penetration increases allowing for successive scanning of the same surface station at different depths. The 800 Hz field strength ratio contour map and 3D surface map show even anomaly distribution similar to the VGM and VLF-EM anomaly maps (Fig. 7). These small elliptical anomalies, uniformly distributed all over the surveyed area, have shallow depths and coincide well with the anomalies appearing on the vertical magnetic gradient and VLF-EM maps. On the light of the geological structures of the area and the quantitative results of the regional survey, five sulfide bodies have been detected in the study area. Each one of these bodies comprises a number of neighboring anomalies that have similar characteristics and may belong to one subsurface body. The interpreted subsurface sulfide bodies are distributed evenly in the study area and trend around the NW-SE direction. Some of the revealed sulfide bodies are displaced by the NE-SW fault system.

This fits well with the geology of the study area since it is a common knowledge that the NW-SE structural trend is older than that of the NE-SW.

The 200 Hz FSR contour and 3D surface maps show gradual decrease in the intensity and amplitude of some anomalies detected using frequency of 800 Hz (Fig. 8) proving that the concentration of the sulfide mineralizations decreases with depth at the peripheral parts of the study area. One anomalous zone, however, remains intact on all frequencies. This is the anomalous zone located near the southcentral part of the highly altered area and coincident with the anomaly detected on the potassium/thorium ratio map (Fig. 6). This may imply that vanishing anomalies around the periphery of the highly altered area are related to shallow sulfide bodies while the persisting group of anomalies in the center of the highly altered area are related to a larger, deeper subsurface sulfide body or a group of closely accumulating bodies. This layout could be also interpreted in the framework of the porphyry copper deposits, where the concentration of the sulfide minerals increases towards the center of the body.

The regional turam survey collected at different depths indicates 2 different subsurface images. The shallow part has a large number of uniformly distributed and of similar value anomalies over the entire area. On the other hand, deeper images show gradual fading away of anomalies covering the margins of the altered area and a clear persistence of the group of anomalies coinciding with the southcentral corner of the altered area.

To further investigate this anomaly or group of anomalies close to the southern corner of the altered area, a second part of the turam field survey is conducted using lowest possible frequency (200 Hz). This survey is conducted using closer profile spacing (50m) and smaller station interval (20m). The main purpose of this detailed survey is to acquire a better view of this anomaly, which would guide the process of constructing a solid conceptual model explaining the mode of occurrence of sulfide mineralization in the area. The detailed 200 Hz field strength ratio contour map confirmed the presence of a semi-rounded, single, large anomaly, whose long axis is parallel to the NW-SE direction (Fig. 9). Moreover, this anomaly is displaced, near its middle, by the NE-SW fault system. The calculated depth to this subsurface sulfide body is 187 m below the ground surface and the estimated conductivity of the subsurface body causing this anomaly is found to be three times larger than the maximum conductivity estimated for shallow anomalies. The drastic contrast in conductivity between this anomaly and shallower anomalies implies that the subsurface bodies causing these anomalies have different sulfide concentrations. The difference in conductivity, shape, and size between these two patterns of anomalies also indicate a different nature of the subsurface bodies causing them.

Integrating the results of the different geophysical methods used to survey the area has led to the construction of a 3D conceptual model that explains the origin and subsurface mode of occurrence of the sulfide mineralization in the surveyed area (Fig. 10). This model suggests that an immense hydrothermal activity has occurred underneath the highly altered area. This migration of a massive pile of hydrothermal solutions has led to the formation of the previously mentioned alteration zones on the surface and to the accumulation of a large body of sulfide mineralization underneath the southcentral part of the highly altered area. This claim is supported by the evidences acquired from both the gamma-ray spectrometry data and the low frequency turam measurements.

The potassium/thorium ratio concentration maps imply the accumulation of both radioelements, most likely due to hydrothermal activities, and leaching of the thorium with time because of its mobility compared to the more stable potassium. This created a semi-circular large anomaly whose peak points to the area underneath which the hydrothermal

activities occur. Another support to this view is the detailed 200 Hz turam survey that confirms the presence of a large elliptical subsurface conductive body at a greater depth and with higher conductivity than the shallow anomalies encountered near the outer borders of the study area.

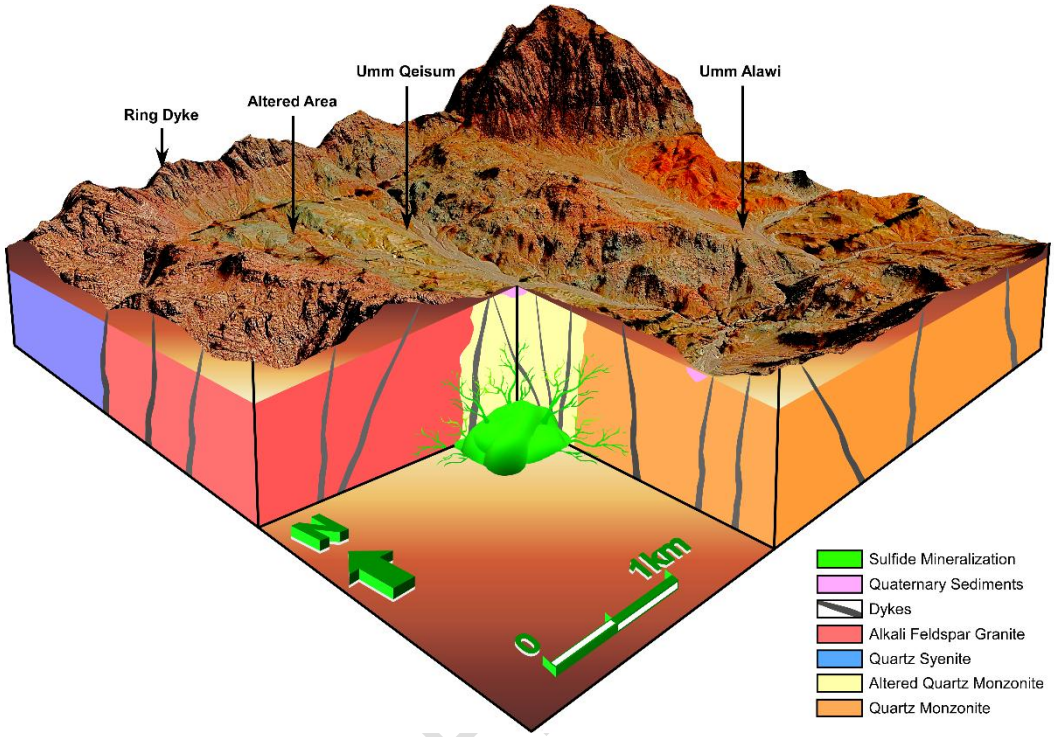

Fig. 10. 3D conceptual model showing the mode of occurrence of subsurface sulfide mineralization in Saint Catherine area

At a later stage, after the hydrothermal solution had lost most of their momentum, some of the hydrothermal residuals managed to find their ways through the weakness zones, such as fault planes and the walls of existing dykes, to accumulate at shallow depths. The fragility of the altered quartz monzonite rocks and the high fractures density in this area might have helped the seepage of hydrothermal solutions through weakness zones and the deposition of sulfide mineralizations along structural lineaments. These accumulations have built up another pattern of sulfide deposits that are randomly distributed all over the area including some in the fresh quartz monzonite rocks. This may explain the small size, shallow depth, weak amplitude, NW-SE alignment, and low conductivity of such anomalies. It also clarifies the irrelevance of these anomalies to the highly altered area. In a later stage, both the deep massive sulfide deposits and the shallow scattered lower concentration deposits are shattered and displaced by the NE-SW fault system. These displacements and grinding of both shallow and deep sulfide deposits along the faulted blocks affected by the NE-SW fault system have added more complication to the current mode of occurrence of sulfide mineralizations in the surveyed area.

5. CONCLUSION

The objective of this integrated geophysical investigation is to solve the debated issue of the origin and mode of occurrence of sulfide mineralizations near the Saint Catherine City. The

integration of the results of geophysical surveys has led to the construction of a solid, evidence-based, and realistic 3D conceptual model that explains the origin, evolution, and current situation of these sulfide mineralizations. The model proposes that hydrothermal solutions has deposited deep massive body of sulfide mineralization underneath the northeastern corner of the quartz monzonite pluton. These hydrothermal solutions created the highly altered area and are responsible for the surface alteration zones. Later, residuals of these hydrothermal solutions managed to travel farther upward assisted by their higher fluidity and the fragility of the altered quartz monzonite rocks, forming a group of shallower, NW-SE trending, randomly distributed small pockets of sulfide mineralizations. Finally, both deep and shallow sulfide mineralizations are affected by the NE-SW trending faults creating a complicated and confusing current situation. This proposed model embraces all available geological, geophysical, and geochemical evidences and solves the tangled debate among researchers about the origin, evolution, and current placement of the sulfide mineralizations in Saint Catherine area.

REFERENCES

1. El-Ghawaby M. Image linear analytical approach to copper mineral exploration in south Sinai, Egypt. Bull Fac Sci Zag Univ. 1984; 6: 55-72.

2. Shendi E. Geophysical investigation of some mineral occurrences in Umm Qeisum Umm Alawi area, south Sinai, Egypt. PhD Dissertation, Suez Canal University. 1988; 109p.

3. Khalifa I. Geochemical orientation survey for copper in Sinai. MSc Dissertation, Suez Canal University. 1991; 106p.

4. Rashed M. Turam electromagnetic investigations on some mineral occurrences of Saint Catherine area, south Sinai, Egypt. MSc Dissertation, Suez Canal University. 1995; 104p.

5. Arnous M. Integrated remote sensing and GIS investigation of mineralizations in Saint Catherine area, South Sinai, Egypt. MSc Dissertation, Suez Canal University. 2000; 121p.

6. Mamoun K, Soliman F, Shendi E, Khalil S, Nakagawa K. Integrated geophysical exploration for sulphide minerals in the Wadi Sa'al area, south Sinai, Egypt. J Geosci, Osaka City Univ. 2004; 47: 113-126.

7. Shendi E, Ismail A, Attia T. On the use of gravity and magnetic anomalies for locating probable areas of metallic mineralization in South Sinai, Egypt. Arab J Geosci. 2008; 1: 137–147. https://doi.org/10.1007/s12517-008-0013-1.

8. Mamedov E, Ahmed E, Chiragov M. Copper–gold–sulphide mineralization associated with late Precambrian volcanic ring structures, Southern Sinai, Egypt. Arab J Sci Eng. 2014; 39: 273–286. https://doi.org/10.1007/s13369-013-0854-0.

9. Shendi E, Aziz A, Mamoun K, Gamal M. The effectiveness of the very low frequency electromagnetic method in the exploration of sulphide mineralization in arid environments, case study from South Sinai Peninsula, Egypt. Environ Earth Sci. 2017; 76: 783. https://doi.org/10.1007/s12665-017-7130-7.

10. El-Agami N. Manganese mineralization related to the Red Sea rift system: examples from the Red Sea Coast and Sinai, Egypt. In: Rasul, N. and Stewart I. (ed) Geological

setting, paleoenvironment and archaeology of the Red Sea, Saudi Geological Survey, KSA. 2019; 473-495. https://doi.org/10.1007/978-3-319-99408-6_21.

11. Abu-Khoziem H. Characterization and leaching potentialities of some rare metals from mineralized rocks, Southern Sinai, Egypt, PhD Dissertation, Cairo University. 2012; 223p.

12. El-Ghawaby M, Hilmy M, El Kaliuby B, Hassan O, Shendi E. Possibilities of porphyry copper mineralization in south Sinai. Proc 2nd Conf Geol Sinai Develop, Suez Canal University. 1989; 2: 59-64.

13. Rabeh T. Tracing the manganese ore accumulations in Sinai Peninsula, Egypt, using magnetic method. Environ Earth Sci. 2016; 75: 228. https://doi.org/10.1007/s12665-015-4966-6.

14. Salem H, Elfouly A. Minerals reconnaissance at Saint Catherine Area, southern central Sinai, Egypt and their environmental impacts on human health. ICEHM 2000, Cairo University. 2000; 586-598.

15. Hassan O. Geology and mineralization of El-Regita area, central south Sinai. MSc Dissertation, Suez Canal University. 1987; 134p.

16. Sharma S, Biswas A, Baranwal V. Very low-frequency electromagnetic method: a shallow subsurface investigation technique for geophysical applications. In: Sengupta, D. (ed) Recent trends in modeling of environmental contaminants. Springer, New Delhi. 2014; 119-141. https://doi.org/10.1007/978-81-322-1783-1_5.

17. Eberle D. A method of reducing terrain relief effects from VLF-EM data. Geoexplor. 1981; 19: 103–114. https://doi.org/10.1016/0016-7142(81)90023-5.

18. Fraser D. Contouring of VLF-EM data. Geophys. 1969, 34: 958–967. https://doi.org/10.1190/1.1440065.

19. Barongo J. Method for depth estimation on aeromagnetic vertical gradient anomalies. Geophys. 1985; 50: 892-1047. https://doi.org/10.1190/1.1441974.

20. Smith R. Some depth formulae for local magnetic and gravity anomalies. Geophys Prospec. 2006; 7:55 – 63. https://doi.org/10.1111/j.1365-2478.1959.tb01453.x.

21. Davis J, Guilbert J. Distribution of the radioelements potassium, uranium, and thorium in selected porphyry copper deposits. Econ Geol. 1973; 68: 145–160. https://doi.org/10.2113/gsecongeo.68.2.145.

22. Cathles L, Shannon R. How potassium silicate alteration suggests the formation of porphyry ore deposits begins with the nearly explosive but barren expulsion of large volumes of magmatic water. Earth Planet Sci Lett. 2007; 262: 92-108. https://doi.org/10.1016/j.epsl.2007.07.029.

23. Watanabe Y, Sato R, Sulaksono A. Role of potassic alteration for porphyry Cu mineralization: implication for the absence of porphyry Cu deposits in Japan. Resour Geol. 2018; 68: 195-207. https://doi.org/10.1111/rge.12165.

24. Duckworth K, Bays A. A modified mode of operation for the turam electromagnetic system with benefits for deep exploration. Geophys Prospect. 1984; 32: 317-335. https://doi.org/10.1111/j.1365-2478.1984.tb00734.x.

25. Duckworth K, O'Neill D. Comparison of scale model results with field surveys conducted over the Night Nawk test range using fixed-loop and moving-source electromagnetic systems. Can Jour Expl Geoph. 1992; 28: 1-5.